JOURNAL OF AGRICULTURAL AND FOOD CHEMISTRY

Article

pubs.acs.org/JAFC

Analysis of Palmitoyl Apo-astaxanthinals, Apo-astaxanthinones, and their Epoxides by UHPLC-PDA-ESI-MS

Yannick Weesepoel,[†,§] Harry Gruppen,[†] Wouter de Bruijn,[†] and Jean-Paul Vincken*[,†]

[†]Laboratory of Food Chemistry, Wageningen University, P.O. Box 17, 6700 AA Wageningen, The Netherlands

[§]FeyeCon Carbon Dioxide Technologies, Rijnkade 17a, 1382 GA Weesp, The Netherlands

Supporting Information

ABSTRACT: Food products enriched with fatty acid-esterified xanthophylls may result in deviating dietary apo-carotenoids. Therefore, free astaxanthin and its mono- and dipalmitate esters were subjected to two degradation processes in a methanolic model system: light-accelerated autoxidation and hypochlorous acid/hypochlorite ($HOCl/OCl^-$) bleaching. Reversed phase ultrahigh-performance liquid chromatography photodiode array with in-line electrospray ionization mass spectrometry (RP-UHPLC-PDA-ESI-MS) was used for assessment of degradation products. Apo-astaxanthinals and -astaxanthinones containing 3 (apo-9) to 10 (apo-8′) conjugated double bonds were found upon autoxidation for all three types of astaxanthin (except free apo-8′-astaxanthinal). Fragmentation of $[M + H]^+$ and $[M + Na]^+$ parent masses of apo-astaxanthins from dipalmitate astaxanthin indicated palmitate esterification. Astaxanthin monopalmitate degradation resulted in a mixture of free and palmitate apo-astaxanthins. $HOCl/OCl^-$ rapidly converted the astaxanthins into a mixture of epoxy-apo-9- and epoxy-apo-13-astaxanthinones. The palmitate ester bond was hardly affected by autoxidation, whereas for $HOCl/OCl^-$ the ester bond of the apo-astaxanthin palmitoyl esters was degraded.

KEYWORDS: *apo-astaxanthins, UHPLC-PDA-ESI-MS, fatty acid ester, xanthophyll, light-accelerated degradation, hypochlorite bleaching*

INTRODUCTION

For many years, the addition of artificially produced carotenoids to food products has been common practice in the food industry. Recent market demands toward natural substitutes have stimulated research on obtaining and utilizing carotenoids of natural origin. Algae, such as *Haematococcus pluvialis*, can be used for producing these natural carotenoids.[1] *H. pluvialis* produces the red carotenoid astaxanthin (3,3′-dihydroxy-*β*,*β*-carotene-4,4′-dione, Figure 1) in 2−3% (w/w) dry weight (dw) quantities. Different from its chemically synthesized astaxanthin analogue, *H. pluvialis* astaxanthin predominantly exists as mono- and diesterified fatty acid forms, 70−90 and 5−25%, respectively.[2,3]

Carotenoids are regarded as powerful antioxidants, which degrade during processing and dietary uptake of foods. This process has been investigated especially for *β*,*β*-carotene. Various types of degradation reactions are associated with food processing and dietary uptake and evidently result in many degradation products.[4] In Figure 1, three reactions, generally known to occur upon carotenoid degradation, are putatively projected on astaxanthin (esters). Cleavage of conjugated double bonds (CDBs) results in a series of apo-astaxanthin (astaxanthins with a shortened carbon skeleton), aldehydes, and ketones (reactions 1, R1a and R1b, respectively). Depending on which CDB is disrupted, a pair of aldehydes (R1a) or a ketone and an aldehyde (R1b) is formed. Epoxidation of the 5−6 CDB of astaxanthin can result in 5,6-epoxy-astaxanthins (reaction 2, R2a). This process can also yield 5,8-furanoid-astaxanthins, which can be formed directly or via acidic rearrangement from the 5,6-epoxide form (R2b). Furthermore, the cleavage of the fatty acid ester might result in free astaxanthin or astaxanthin monoester (reaction 3, R3). Finally, the degradation products resulting from R1, R2, and R3 can undergo additional degradation via R1 or R2, until they end up as structures with little resemblance to the original carotenoid.[4−8] Also, *cis*−*trans* isomerization might be regarded as a degradation reaction,[4] but is not further considered here.

A common carotenoid degradation reaction that results in R1 and R2 degradation products is oxidation. A relatively mild form of oxidation, occurring during product processing and storage, is autoxidation. This reaction can occur spontaneously and is accelerated by light sensitization, oxygen, and/or elevated temperatures. During autoxidation the CDBs of the carotenoid chromophore are reduced or cleaved, resulting in numerous products. Autoxidation is generally believed to proceed via carbon−peroxyl triplet radicals, which propagate the reaction via intramolecular homolytic substitution.[9] In contrast, a relatively aggressive oxidative agent is hypochlorous acid (HOCl). In the human body, HOCl can be formed upon inflammatory reactions by the enzyme myeloperoxidase in polymorphonuclear leukocytes.[10] There, HOCl is primarily produced to eliminate harmful bacteria or toxins, but it is also known to damage surrounding tissue.[11,12] Also, the dietary carotenoids present in the bloodstream[13,14] can be converted by HOCl into oxidation products that might be toxic.[15,16] HOCl occurs in equilibrium with its corresponding base OCl^-, and together they are referred to as $HOCl/OCl^-$ or

Received: July 23, 2014
Revised: September 24, 2014
Accepted: October 1, 2014
Published: October 3, 2014

dx.doi.org/10.1021/jf503520q | J. Agric. Food Chem. 2014, 62, 10254−10263

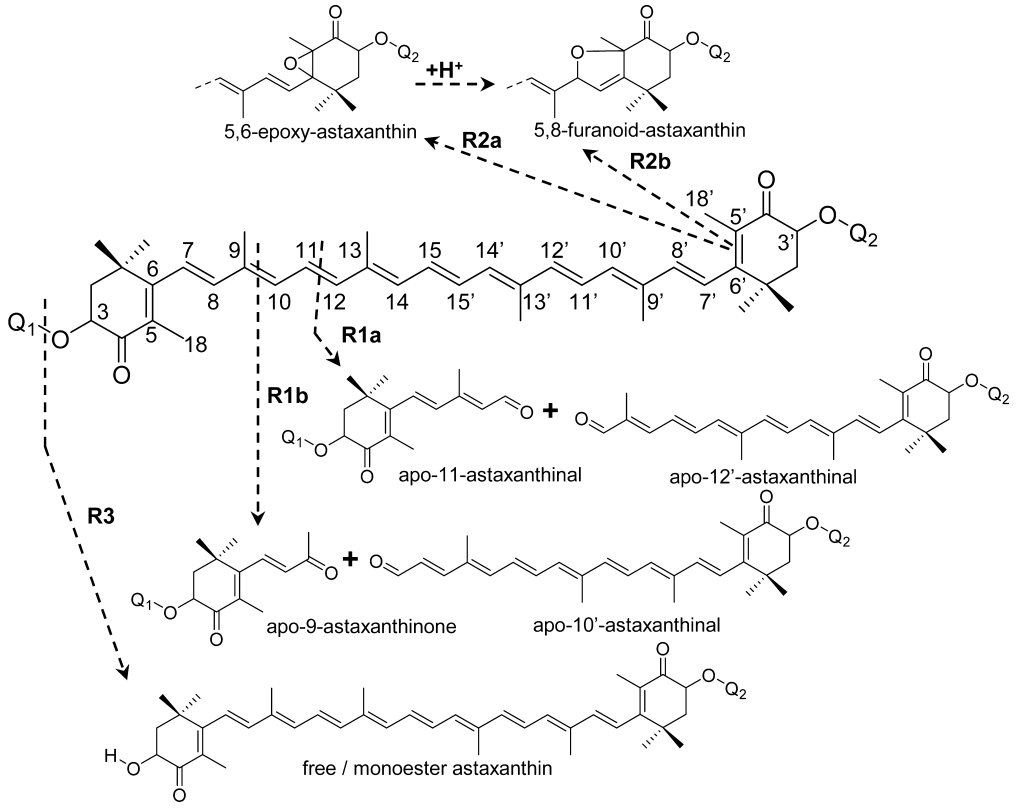

Figure 1. Chemical structures of astaxanthin and examples of degradation reactions and products. Reaction 1 (R1a and R1b) CDB cleavage; reaction 2 (R2a and R2b), 5,6-epoxide and 5,8-furanoid formation; reaction 3 (R3), de-esterification. Free astaxanthin, $Q_1 = Q_2 = H$; astaxanthin monopalmitate, $Q_1 = (C{=}O){-}C_{15}H_{31}$ and $Q_2 = H$; astaxanthin dipalmitate, $Q_1 = Q_2 = (C{=}O){-}C_{15}H_{31}$.

hypochlorite. The reaction products formed from *β,β*-carotene by hypochlorite bleaching were *β*-apo-13-carotenone, *β*-apo-15-carotenal, and *β*-apo-14′-carotenal. Furthermore, smaller volatiles derived from C7−C8 (e.g., *β*-cyclocitral) and C9−10 (e.g., *β*-ionone, dihydroactinidiolide) cleavages were found.[17,18]

Unlike *β,β*-carotene, xanthophylls (oxygenated carotenoids), comprising, among others, astaxanthin, canthaxanthin, lutein, and zeaxanthin, have not gained much attention, with respect to neither autoxidation nor hypochlorite bleaching. Furthermore, the fate of the fatty acid ester has not been assessed. For hypochlorite bleaching, it has been reported that the xanthophylls lutein, zeaxanthin, *α*-cryptoxanthin, (*β*-)-cryptoxanthin, and anhydrolutein were degraded, but no reaction products were described.[19] Upon oxidation of canthaxanthin by nickel peroxide, mainly apo-canthaxanthinals and canthaxanthinones were found.[20] It was also shown that upon autoxidation of free astaxanthin a series of apo-astaxanthinals and -astaxanthinones were found with apo-13-astaxanthinone as the main reaction product.[21] Treatment by peroxynitrite resulted in a mixture of apo-astaxanthins and nitro-astaxanthins.[22] The stability of the ester bond connecting astaxanthin and a fatty acid has never been assessed using light-accelerated autoxidation or hypochlorite bleaching, although the deliberate removal of the fatty acid by means of methanolic saponification and lipases has been reported.[23,24]

As a consequence of esterfication with fatty acids, the number of potential xanthophyll oxidative degradation products is expected to be larger than that for nonesterified xanthophylls. Therefore, this study reports on the analysis of apo-astaxanthin mixtures using a new method comprising reversed phase ultrahigh-performance liquid chromatography (RP-UHPLC) in combination with in-line electrospray ionization mass spectrometry (ESI-MS). For triggering the formation of reaction products through the various routes R1a, R1b, R2a, R2b and R3, light-accelerated autoxidation and hypochlorite bleaching were performed on astaxanthin, astaxanthin monopalmitate ester, and astaxanthin dipalmitate ester. The experiments were performed in pure solvent to minimize matrix effects.

MATERIALS AND METHODS

Materials. (3*RS*)-Apo-12′-astaxanthinal (>98% w/w), (3*RS*,3′*RS*)-astaxanthin (97% w/w), (3*RS*,3′*RS*)-astaxanthin monopalmitate (97% w/w), and (3*RS*,3′*RS*)-astaxanthin dipalmitate (98% w/w) were purchased from CaroteNature (Lupsingen, Switzerland). ULC-MS grade methanol absolute (≥99.9% w/w), acetonitrile (≥99.9% w/w), water and formic acid (99% w/w), AR grade ethyl acetate (99.8% w/w), and HPLC grade chloroform (≥99.9% v/v, corrected for stabilizer, stabilized by 0.5−1.5% (w/v) ethanol) were purchased from Biosolve (Valkenswaard, The Netherlands). Sodium hypochlorite solution (active Cl 12.3−14.9% w/v) in H_2O was purchased from Carl Roth (Karlsruhe, Germany).

Preparation of Carotenoid Stock Solutions. Apo-12′-astaxanthinal, free astaxanthin, astaxanthin monopalmitate, and astaxanthin dipalmitate were separately dissolved in chloroform. All stock solution concentrations were determined spectrophotometrically in hexane/chloroform (minimum 98% (v/v) *n*-hexane). Astaxanthin concentrations were determined at 470 nm using the absorption coefficient $A^{1\%}_{1\ cm}$ of 2100 L g^{-1} cm^{-1}.[25] For astaxanthin monopalmitate and dipalmitate, concentrations were subsequently corrected for the difference in molecular weight, assuming that the fatty acid moiety did not contribute to absorption, yielding values of $A^{1\%}_{1\ cm}$ of 1501 and 1167 L g^{-1} cm^{-1}, respectively. For apo-12′-astaxanthinal, concentrations were determined at 421 nm using $A^{1\%}_{1\ cm}$ of 2276 L g^{-1} cm^{-1}.[26]

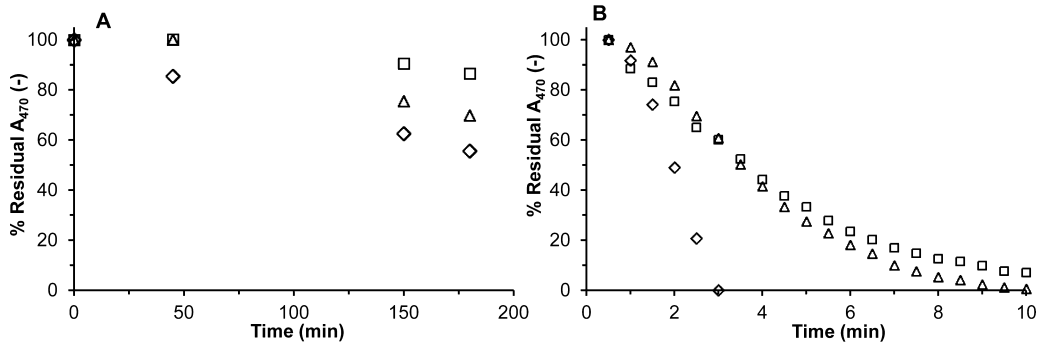

Figure 2. Decrease in visible absorption of various astaxanthins subjected to (A) light-accelerated autoxidation and (B) hypochlorite bleaching over time at 470 nm followed by spectrophotometry: free astaxanthin (□); astaxanthin monopalmitate (△); astaxanthin dipalmitate (◇).

Light-Accelerated Autoxidation. Free astaxanthin, astaxanthin monopalmitate, and astaxanthin dipalmitate were separately diluted in methanol to concentrations of 18.0, 19.6, and 24.0 μM, respectively. Aliquots (1.5 mL) were transferred to quartz cuvettes (type 114-QS, Hellma Analytics, Müllheim, Germany) closed with stoppers. A headspace of approximately 50 μL was left, filled with atmospheric air. Three cuvettes for each type of astaxanthin were irradiated for 3 h in a Suntest XLS+ (Atlas MTS, Chicago, IL, USA) equipped with a 1700 W xenon arc lamp and window glass filter. Irradiation energy was set to 30 W m^{-2}, and black standard temperature was maintained at 79 °C, which corresponded to a methanol sample temperature of 55 °C. The triplicates were pooled per type of astaxanthin and evaporated to dryness under a stream of nitrogen. Next, samples were redissolved in ethyl acetate and subsequently supplemented with acetonitrile to reach a ratio of ethyl acetate/acetonitrile 1:3 (v/v). Prior to UHPLC injection, samples were filtered using Whatman Rezist 13 0.45 μm PTFE syringe filters (GE Life Sciences, Fairfield, CT, USA).

Hypochlorite Bleaching. Bleaching of astaxanthin with hypochlorite was adapted from ref 15. Free astaxanthin, astaxanthin monopalmitate, and astaxanthin dipalmitate were diluted in 900 μL of methanol to concentrations of 30.3, 32.9, and 40.4 μM, respectively. Subsequently, degradation was carried out by the addition of 65 μL of approximately 12% (w/v) NaOCl solution and incubation for 10 min at room temperature in daylight. Estimation of the decrease in absorbance at 470 nm in time was made by comparison with a methanol/hypochlorite blank. Subsequently, the methanol layer was extracted three times using 900 μL of *n*-hexane each time. The *n*-hexane layers were pooled and evaporated to dryness under a stream of nitrogen in the dark. Rearrangement of 5,6-epoxides into 5,8-furanoids was performed by dissolving the evaporated hexane layer in 2.0 mL of 100% (v/v) ethanol. Eight hundred microliters of the ethanol-resolved degradation products was acidified with 50 μL of 0.1 M HCl.[27,28] Prior to UHPLC analysis, samples were prepared as for light-accelerated autoxidation.

RP-UHPLC-PDA-ESI-MS Analysis of Degradation Products. Separation and identification of carotenoid degradation products were carried out using a Thermo Accela UHPLC system (Thermo Scientific, San Jose, CA, USA) equipped with a pump, degasser, autosampler, and photodiode array (PDA) detector and coupled in-line to a LTQ-Velos double ion trap mass spectrometer equipped with a heated ESI probe (Thermo Scientific). Samples were injected onto an Acquity UPLC BEH Shield RP18 column (2.1 × 150 mm, 1.7 μm particle size; Waters, Milford, MA, USA) fitted to a Vanguard precolumn (2.1 × 5 mm, 1.7 μm particle size; Waters). The flow rate was 300 μL min^{-1}, operated at 23 °C. The eluents used were the following: 1% (v/v) acetonitrile in Millipore water (A), acetonitrile (B), and ethyl acetate (C), all containing 0.10% (v/v) formic acid as a mobile phase modifier. The elution program was started from 95% (v/v) A/5% (v/v) B and followed by 0−20 min linear gradient to 100% (v/v) B, 20−25 min isocratic at 100% (v/v) B, 25−32 min linear gradient to 100% (v/v) C, and 32−35 min isocratic at 100% (v/v) C. The eluent was adjusted to its initial composition in 10 min, followed by equilibration for 5 min. Detection wavelengths for UV−vis were set at 280 ± 0.5, 370 ± 0.5, and 450 ± 0.5 nm. Data were recorded at 10 Hz.

Mass spectrometric data were recorded in positive ion mode. Nitrogen was used as both sheath (30 arbitrary units) and auxiliary gas (10 arbitrary units). Settings of the mass spectrometer were tuned by 3 μL min^{-1} direct injection of apo-12′-astaxanthinal in a mixture of ethyl acetate/acetonitrile 1:3 (v/v). Most settings were optimized via automatic tuning by using LTQ Tune Plus 2.7 (Thermo Scientific). The temperature of the ion transfer tube was 450 °C and the source voltage, 3.5 kV. Data were recorded over the *m*/*z* segments 150−350 (0.50−10.00 min), 250−500 (10.00−15.40 min), 350−500 (15.40−19.00 min), 420−680 (19.00−23.00 min), 400−575 (23.00−24.40 min), 400−590 (24.40−24.95 min), 542−650 (24.95−26.80 min), 615−720 (26.80−29.30 min), and 615−1250 (29.30−37.00 min). Within these segments dynamic data-dependent MS^2 fragmentation was performed on the most intense parent ion (x = 1) and subsequently on the second most intense parent (x = 2). Dynamic exclusion was used to identify coeluting apo-astaxanthins. Also, it served the purpose of fragmenting both $[M + H]^+$ and $[M + Na]^+$ spectra within one chromatographic peak. A repeat count of two MS^2 spectra per parent ion and a maximum of x = 25 or within a time frame of 5.0 s were used as settings. The collision-induced dissociation was set to 35%. Data acquisition and reprocessing were done with Xcalibur 2.2 (Thermo Scientific).

RESULTS AND DISCUSSION

Time Course of Color Loss of Various Astaxanthins. The astaxanthin degradation was performed by light-accelerated autoxidation via exposure to high-intensity light conditions and elevated temperatures. Conventional autoxidation in darkness at lower temperatures could take up to several weeks.[29] Exposure of the parental *all-trans* forms of the three types of astaxanthin to light-accelerated autoxidation decreased the absorption at 470 nm (Figure 2A). After 180 min of exposure, a decrease of 13% for the free astaxanthin was observed, 30% of the monoester, and 44% of the diester. Subsequently, UHPLC-PDA-ESI-MS was used to assess the degradation products formed. As it is known that β,β-carotene forms small volatile compounds upon extensive degradation,[8,9] our degradation experiments were terminated with a high proportion of residual parent material, so that an overview of intermediate degradation products would be obtained. After 45 min, the absorption of the free astaxanthin and monoester was not reduced (Figure 2A). Their absorption spectra showed only a hypsochromic shift of 3−5 nm (data not shown). In contrast, the diester already showed a decrease in A_{470} of 14% within 45 min. This indicated that esterification can influence color stability, which has also been reported before.[30,31]

The three types of astaxanthin were also exposed to bleaching with astaxanthin/HOCl ratios in the range of 1:3.5

and 1:5.0 (mol/mol). These ratios were reported to occur (locally) in inflamed tissues in the body.[18] The three types of astaxanthins all showed a ~100% decrease in A_{470} upon bleaching, within 10 min (Figure 2B). This indicated that the reaction approached the end-point. No noticeable differences in stability between the free and monopalmitate astaxanthin degradation were observed, whereas the dipalmitate astaxanthin showed a more rapid degradation, as was also observed with light-accelerated autoxidation. No plausible explanation for this difference could be provided. Due to the different nature of the light-accelerated autoxidation and hypochlorite bleaching, they resulted in different sets of degradation products, which were used to design the LC-MS analysis method.

Free Apo-astaxanthinals and Apo-astaxanthinones (R1a, R1b). The absorbance maxima of the various degradation products of astaxanthin (esters) are expected to be related to the number of CDBs present in the molecules. To detect the widest array of apo-astaxanthins possible by PDA, detection wavelengths were set at 450, 370, and 280 nm. Using these three wavelengths, upon light-accelerated autoxidation a plethora of peaks was found, of which 44 could be tentatively annotated (Figure 3 and Table 1). Free apo-astaxanthinals and -astaxanthinones were found at different detection wavelengths and eluted between approximately 7.0 and 18.0 min. For the astaxanthin dipalmitate samples no PDA response was observed, indicating that no free apo-astaxanthinals and -astaxanthinones were formed. A first ascertainment of the apo-astaxanthinals and -astaxanthinones was done by locating their predicted m/z values with the full scan MS data accompanying a chromatographic peak (Table 1). Using this approach, the matching protonated parent masses ($[M + H]^+$) for apo-9- and apo-13-astaxanthinone and apo-11-, apo-15-, apo-14′-, apo-12′-, and apo-10′-astaxanthinal were found upon treatment of both free and monopalmitate astaxanthin. The accompanying absorption spectra of these apo-astaxanthins had increasing λ_{max} values from apo-9-astaxanthinone (260−270 nm) to apo-10′-astaxanthinal (452 nm). The smallest aldehyde, apo-7-astaxanthinal, was probably also formed. However, our approach will not visualize this compound due to its limited conjugated system or likely volatile properties. Nevertheless, the MS trace showed $[M + H]^+$ (m/z 183) values that could potentially be associated with apo-7-astaxanthinal, but no diagnostic MS^2 fragments could be obtained for a reliable annotation.

The identification was further verified by analyzing MS^2 fragmentation of all $[M + H]^+$ parents annotated and comparison with the MS^2 spectrum of the apo-12′-astaxanthinal standard, which had retention time, parent mass, and MS^2 fragmentation similar to those of the apo-12′-astaxanthinal formed (peak 12) in our degradation study. The MS^2 spectra of the apo-astaxanthinals and -astaxanthinones all showed similar fragmentation behavior upon CID fragmentation (Supporting Information Table S1). In Figure 4A fragmentation of apo-12′-astaxanthinal is displayed as an example. The most intense neutral loss in the MS^2 spectra of the free apo-astaxanthinals and -astaxanthinones was 18 Da, yielding the fragment m/z 363.2. The loss originates from the hydroxyl group at C3, analogous to water neutral loss with the (native) astaxanthin molecule.[32] The second water loss, yielding the fragment with m/z 345.1, might have originated from the loss of the aldehyde group at C12′. An exception to this dominant water loss was found for apo-11-astaxanthinal, which showed a neutral loss of 42 Da (m/z 205) as the main fragment. This preference for

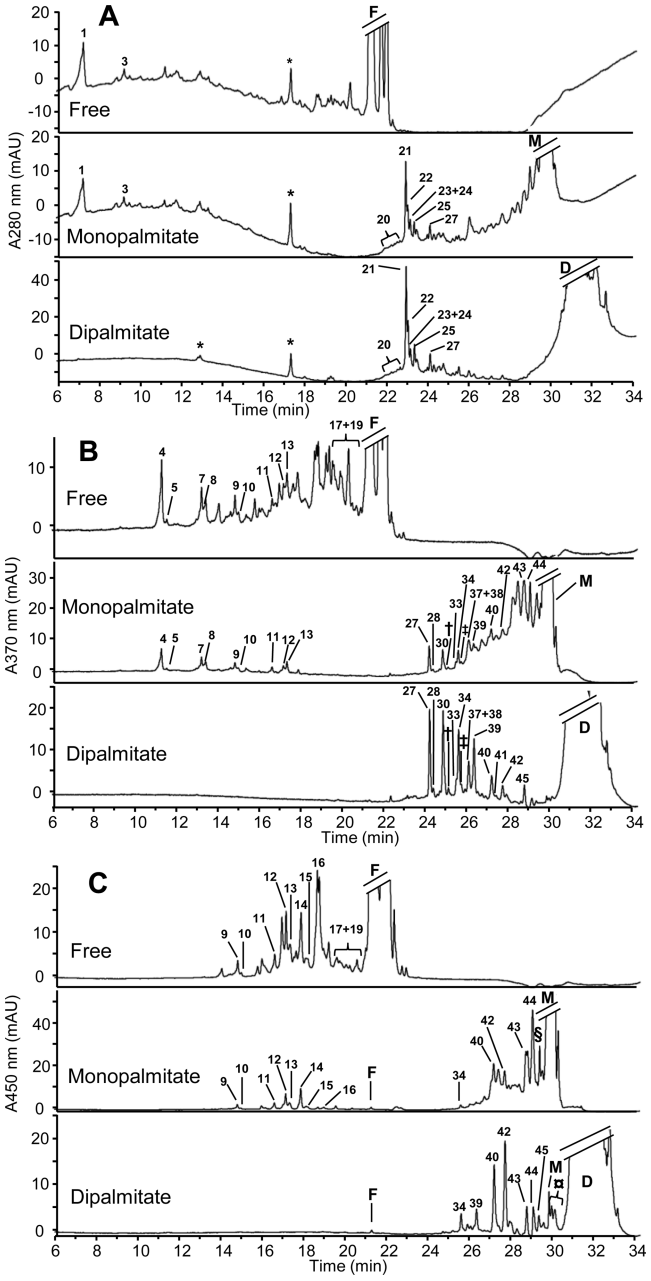

Figure 3. RP-UHPLC-UV chromatograms of free astaxanthin, its monoester, and its diester in methanol after 3 h of light-accelerated degradation: (A) 280 nm; (B) 370 nm; (C) 450 nm. F, free *all-trans*- and *cis*-astaxanthin; M, *all-trans*- and *cis*-astaxanthin monoester palmitate; D, *all-trans*- and *cis*-astaxanthin diester palmitate; ∗, ghost peak; †, peak 29; ‡, peak 34; §, peaks 46, 47, and 48; ¤, peaks 49, 50, and 51.

ejecting 42 Da instead of 18 Da could not be explained. CID fragmentation of $[M + H]^+$ apo-12′-astaxanthinal, and all of the other free apo-astaxanthin aldehydes and ketones described, resulted in a multitude of smaller fragments, typical for carotenoids.[7] In our study, these smaller mass fragments at, for example, m/z 201, 187, 185, 173, 161, 157, 147, 145, 135, 133, and 119 could be interpreted similarly as for apo-carotenals and -carotenones derived from β,β-carotene upon EI-MS, in which a saturated carbon−carbon bond is fragmented and the molecular ion is rearranged. A series of polyene fragmentations and tandem rearrangements resulted in multiple

Table 1. Apo-astaxanthins and Epoxy-astaxanthins Formed during Light-Accelerated Autoxidation and Hypochlorite Degradation of Free Astaxanthin, Astaxanthin Monopalmitate, and Astaxanthin Dipalmitate Tentatively Assigned by UHPLC-ESI-MS[a]

no.	Rt (min)	identification[b]	method[c]	UV−vis$_{max}$ (nm)	$[M + H]^+$, $[M + Na]^{\pm}$ (m/z)
		Apo-astaxanthin Ketones			
1	7.30	apo-9-astaxanthinone	L	260−270	223.1
22	22.98	apo-9-astaxanthinone PE	L	260−270[d]	461.3, 483.3
23	23.10	apo-9-astaxanthinone PE	L, H	260−270[d]	461.3, 483.3
4	11.24	apo-13-astaxanthinone	L, H	345	289.1
5	11.49	apo-13-astaxanthinone	L	345	289.2
27	24.05	apo-13-astaxanthinone PE	L, H	340	527.4, 549.4
28	24.22	apo-13-astaxanthinone PE	L	330	527.4, 549.4
		Apo-astaxanthin Aldehydes			
20	21.81−22.39[e]	apo-7-astaxanthinal PE	L	<260	421.2, 443.1
3	9.27	apo-11-astaxanthinal	L, H	300−305	249.1
24	23.10	apo-11-astaxanthinal PE	L, H	260−270[d]	487.3, 509.3
25	23.29	apo-11-astaxanthinal PE	L, H	313	487.3, 509.3
7	13.15	apo-15-astaxanthinal	L, H	381	315.2
8	13.27	apo-15-astaxanthinal	L, H	363	315.2
30	24.69	apo-15-astaxanthinal PE	L, H	377	553.4, 575.4
31	24.94	apo-15-astaxanthinal PE	L, H	380−390[d]	553.4, 575.4
9	14.75	apo-14′-astaxanthinal	L, H	414	341.2
10	14.92	apo-14′-astaxanthinal	L, H	403	341.2
34	25.43	apo-14′-astaxanthinal PE	L, H	398[d]	579.4, 601.4
35	25.54	apo-14′-astaxanthinal PE	H	397	579.4, 601.4
37	25.91	apo-14′-astaxanthinal PE	L	342[d]	579.4, 601.4
12	17.07	apo-12′-astaxanthinal	L, H	429	381.2
40	27.01	apo-12′-astaxanthinal PE	L, H	430	619.4, 641.4
41	27.23	apo-12′-astaxanthinal PE	H	412	619.4, 641.4
14	17.78	apo-10′-astaxanthinal	L	452	407.2
15	18.05	apo-10′-astaxanthinal	L	410	407.2
42	27.54	apo-10′-astaxanthinal PE	L	449	645.4, 667.5
44	28.88	apo-8′-astaxanthinal PE	L	450	685.4
45	29.15	apo-8′-astaxanthinal PE	L	440	685.4
2	8.71	**Epoxy-apo-astaxanthin Ketones** epoxy-apo-9-astaxanthinone	H	268−271	239.1
21	22.89	epoxy-apo-9-astaxanthinone PE	L, H	260−270[d]	477.2
26	23.37	epoxy-apo-9-astaxanthinone PE	H	260−270[d]	477.3
6	12.83	epoxy-apo-13-astaxanthinone	H	336	305.1
29	24.67	epoxy-apo-13-astaxanthinone PE	H	335	543.4, 565.3
		Epoxy-apo-astaxanthin Aldehydes			
32	25.31	epoxy-apo-15-astaxanthinal PE	H	393	569.4
36	25.56	epoxy-apo-15-astaxanthinal PE	L	401[d]	569.4
38	25.91	epoxy-apo-15-astaxanthinal PE	L	342[d]	569.4
13	17.24	epoxy-apo-12′-astaxanthinal	L	409	397.2
39	26.15	epoxy-apo-12′-astaxanthinal PE	L	394	635.4
43	28.58	epoxy-apo-12′-astaxanthinal PE	L	420	635.4, 657.4
		Epoxy-astaxanthins			
17	18.00−20.50[e]	epoxy-astaxanthin	L	ND[f]	613.3
18	18.00−20.50[e]	diepoxy-astaxanthin	L	ND[f]	629.3
19	18.00−20.50[e]	triepoxy-astaxanthin	L	ND[f]	645.3
46	29.30−29.60[e]	epoxy-astaxanthin PE	L	400	851.6, 873.7
47	29.30−29.60[e]	diepoxy-astaxanthin PE	L	ND[f]	889.5
48	29.30−29.60[e]	triepoxy-astaxanthin PE	L	ND[f]	905.5
49	30.60−31.10[e]	epoxy-astaxanthin diPE	L	ND[f]	1089.8
50	30.60−31.10[e]	diepoxy-astaxanthin diPE	L	ND[f]	1106.7
51	30.60−31.10[e]	triepoxy-astaxanthin diPE	L	ND[f]	1143.8
		Other Apo-astaxanthins			
33	25.34	epoxy-apo-15-astaxanthinoic acid PE	L	400[d]	585.4, 607.4
11	16.53	apo-12′-astaxanthinoic acid	L	414	397.2
16	18.65	apo-8′-astaxanthinol	L	425	449.2

[a]Degradation products are divided into classes and sorted from smallest carotenoid backbone upward. Underlined parent masses were in the $[M + Na]^+$ ionization state. Peak numbers refer to Figures 3 and 6. Additional MS^2 fragmentation data are given in Tables S1 and S2 of the Supporting Information. [b]Epoxides can be either in the 5,6 or 5,8 configuration. PE, palmitate ester; diPE, dipalmitate ester. [c]L, light-accelerated autoxidation; H, hypochlorite bleaching. [d]Mixture of visible spectra due to coelution. [e]No accurate retention time could be determined. [f]ND, not determined.

dx.doi.org/10.1021/jf503520q | J. Agric. Food Chem. 2014, 62, 10254−10263

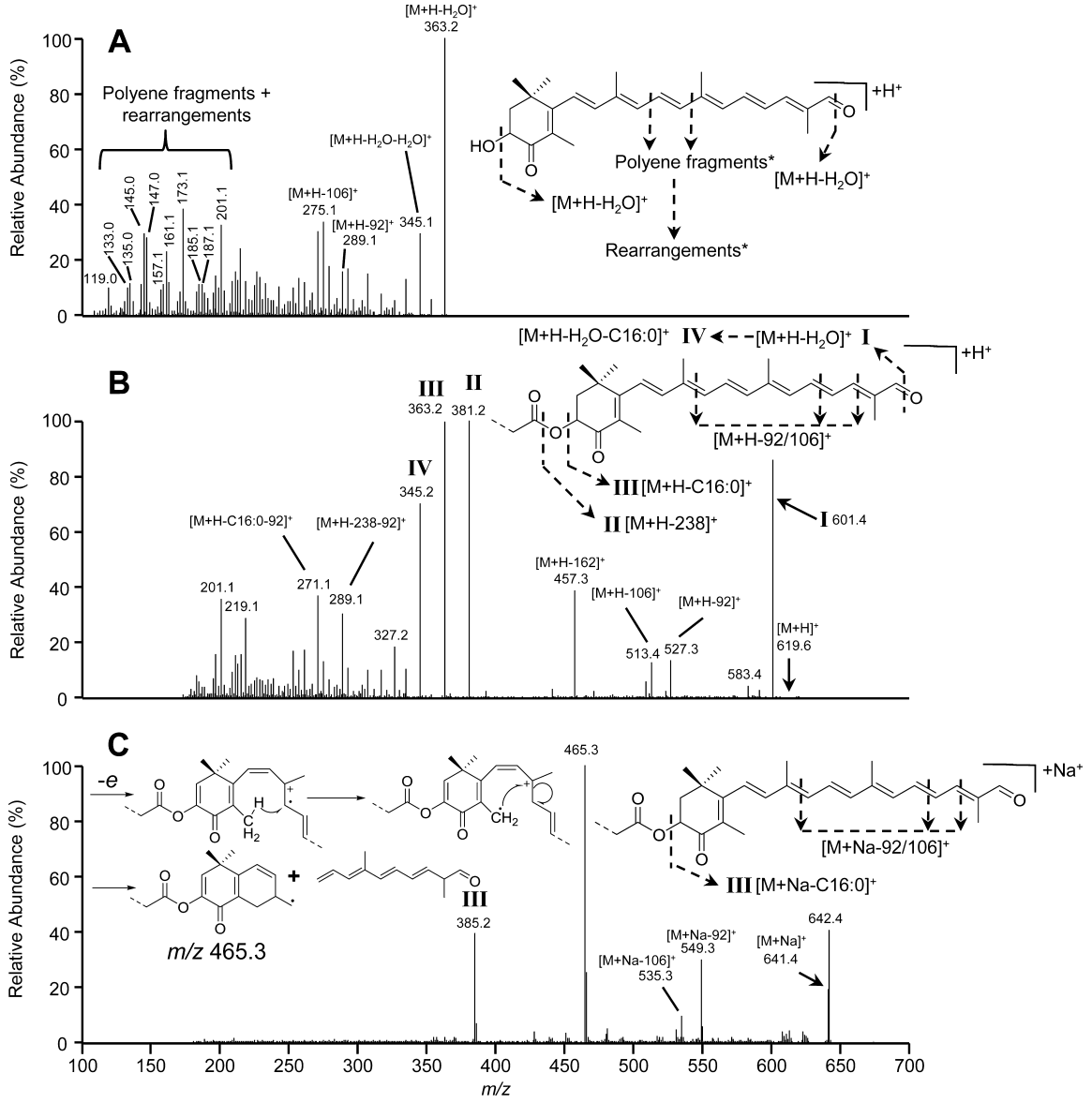

Figure 4. (A) MS^2 spectrum of $[M + H]^+$ apo-12′-astaxanthinal; (B) MS^2 spectrum of $[M + H]^+$ apo-12′-astaxanthinal palmitate ester; (C) MS^2 spectrum of $[M + Na]^+$ apo-12′-astaxanthinal palmitate ester. ∗, examples; fragmentation can occur at multiple C−C bonds in the polyene moiety. Roman numerals refer to MS^2 fragments in Supporting Information Table S2.

ejections of CH_4 and CH_2, giving rise to this wide array of smaller MS^2 fragment ions.[7] Fragments resulting from toluene and xylene polyene elimination products were low in abundance and could in the case of apo-12′ astaxanthinal be annotated to m/z 289.1 and 275.1. Other fragment ions could not be rerouted to a fragmentation of the parent ion.

Apo-astaxanthinal and Apo-astaxanthinone Palmitate Esters (R1a, R1b). When astaxanthin monopalmitate and dipalmitate were subjected to light-accelerated autoxidation, additional peaks appeared in the hydrophobic region of the chromatogram (21.5−30 min) (Figure 3). Again, a first annotation was performed by tracing their respective parent masses (Table 1). Upon assessment of the UV−vis absorption spectra of the peaks, a similar trend was observed as for the free apo-astaxanthinals and -astaxanthinones (Figure 5). The absorption maxima slightly deviated from previously reported λ_{max} values of purified free apo-astaxanthinals and -astaxanthinones (1−14 nm), possibly due to the use of the different LC solvents and coelution with other reaction products.[21] This led to the conclusion that a series of apo-9- to apo-8′-astaxanthinals and -astaxanthinones palmitate esters were formed.

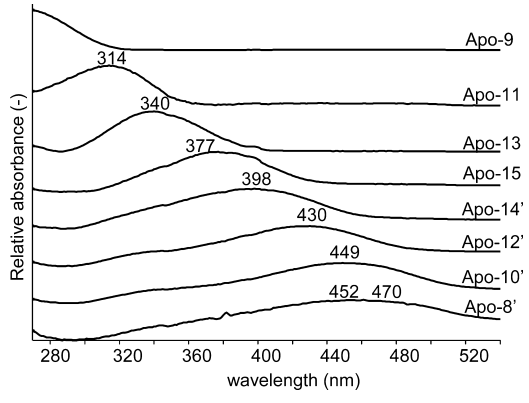

Figure 5. Overlay of UV−vis absorbance spectra of several apo-astaxanthin palmitate ester ketones and aldehydes.

dx.doi.org/10.1021/jf503520q | J. Agric. Food Chem. 2014, 62, 10254−10263

Similar to the astaxanthin esters, MS^2 spectra were used to identify the apo-astaxanthin backbone and the esterified fatty acid (Supporting Information Table S2).[32] As an example, the fragmentation of $[M + H]^+$ apo-12′-astaxanthinal palmitate (peak 40) is explained (Figure 4B). Again, water loss, yielding fragment m/z 601.4 (**I**) was observed, but this time resulting from the aldehyde or ketone group. Most abundant were the fragments at m/z 381.2 (**II**), representing the apo-12′-astaxanthinal backbone, and m/z 363.2 (**III**), which represented the apo-astaxanthin that ejected C16:0. The typical polyene elimination products toluene (92 Da) and xylene (106 Da) were found at m/z 527.3 and 513.4, respectively, albeit in low intensities. Toluene and xylene neutral losses were formed only for apo-12′-astaxanthins and larger apo-astaxanthins and not for the smaller ones. Furthermore, tandem losses of water and palmitate yielded the fragment at m/z 345.2 (**IV**). Also, tandem losses of palmitate ketene and toluene (yielding m/z 289.1) and palmitate and toluene (yielding m/z 271.1) were observed. Contrary to the free apo-7-astaxanthinal, molecular ions of the palmitate ester of apo-7-astaxanthinal (peak 20) could be detected between Rt values of 21.8 and 22.4 min. Upon fragmentation of both the $[M + H]^+$ and $[M + Na]^+$ parents (m/z 421.2 and 443.1, respectively), diagnostic fragments **I**, **II**, and **III** could be annotated (Supporting Information Table S2).

As an additional confirmation of the apo-astaxanthinal and -astaxanthinone palmitoyl structures, esterified astaxanthin sodium adducts $[M + Na]^+$ were analyzed. It has been shown that upon fragmentation, the MS^2 of sodiated ions strongly deviated from the protonated MS^2 fragmentation.[32,33] This was also the case for apo-astaxanthin palmitate esters as shown in Figure 4C. No fragments similar to **II** were found in this case; only the palmitate loss **III** is visible at m/z 385.2 (for apo-7-astaxanthinal and apo-9-astaxanthinone a neutral loss of 238 Da was visible). The main fragment at m/z 465.3 represented a sodiated benzonium ion and could be explained, similarly as for astaxanthin esters, by ring closure at C18 to C9 after electron rearrangement at C5−C6 (Figure 4C inset).[33,34] Remarkably, the formation of this benzonium ion was dominant over the other fragments and could already be observed with apo-9-astaxanthinone. As the sodiated parent mass of apo-9-astaxanthinone is m/z 483.3, one might argue that the m/z 465.4 fragment represents a simple water loss.

Other Apo-astaxanthins and *cis*-Apo-astaxanthins (R1a, R1b). Besides aldehyde and keto functional groups, we also screened for apo-astaxanthinols and apo-astaxanthinoic acids. Only one apo-astaxanthinol could be annotated. Instead of the parent mass of apo-8′-astaxanthinal, an m/z of 449.2 was detected, suggestive for apo-8′-astaxanthinol (peak 16, Table 1 and Figure 3C). The presence of a C7−C8 CDB apo-8′-degradation product indicated that probably the corresponding apo-7-astaxanthin was also formed.

In Table 1, it can be observed that similar apo-astaxanthinal or -astaxanthinone structures were annotated to multiple chromatographic peaks (e.g., peaks 4/5, 7/8, 9/10, 14/15, and 39/43). Probably these represented different *cis*-apo-astaxanthin geometrical isomers. As also *cis*-isomers were formed from *all-trans*-astaxanthin (results not shown), this conclusion seems plausible. Assignment of the geometrical isomers using blue shifts in λ_{max} compared to the *all-trans* isomer is common practice. As these compounds were present in trace amounts, and because it was not always possible to baseline separate degradation products to obtain a spectrum representing a single compound, *cis* and *all-trans* annotations were not pursued.

Epoxy-astaxanthins (R2a, R2b). The formation of epoxides was observed for intact astaxanthin (esters) upon light-accelerated degradation (Table 1). For the free astaxanthin, parent masses associated with mono-, di-, and triepoxides (e.g., epoxides on the C5−C6, C5′-C6′, and C15−C15′ positions) were found (peaks 17−19), eluting together with a plethora of other components just before the free astaxanthin peak F at 370 nm (Figure 3B). Presumably, the astaxanthin epoxides were also visible at 450 nm (Figure 3C), because epoxides normally show a small hypsochromic shift compared to astaxanthin, as will be elaborated later. Fragmentation of the epoxides showed two consecutive water losses and again a multitude of smaller fragments, the most intense of which were annotated in Tables S1 and S2 of the Supporting Information. Most likely, the epoxide groups were in the 5,6-epoxide or the 5,8-furanoid position, reported predominant in autoxidation of β,β-carotene.[5,9] When the carotenoid's C5−C6 and C5′-C6′ positions are occupied with epoxides, a third epoxide group might, for example, be located at the 15−15′ position.[9] Similarly, mono-, di-, and triepoxides were found for astaxanthin monopalmitate (peaks 46−48) and dipalmitate (peaks 49−51) (Table 1; Figure 3B,C). Also for the monopalmitate, the formation of intact astaxanthin epoxides upon autoxidation was observed as a large hump, which made it difficult to pinpoint exact retention times.

Epoxy-apo-astaxanthinones and -astaxanthinals (R1a, R1b, R2a, R2b). Two abundant free apo-astaxanthins, which were found upon hypochlorite degradation of free astaxanthin, its monopalmitate, and its dipalmitate, had parent masses of m/z 239.1 and 305.1. These corresponded to the masses of epoxy-apo-9-astaxanthinone (peak 2) and epoxy-apo-13-astaxanthinone (peak 6), respectively (Table 1; Figure 6). Furthermore, for the astaxanthin monopalmitate and dipalmitate, the esterified forms of the epoxy-apo-9-astaxanthinone with m/z 477.3 (peak 26) and epoxy-apo-13-astaxanthinone with m/z 543.4 (peak 29) were annotated. Following the identification strategy used throughout this study, the epoxy palmitate ester species were identified by fragments **II** and **III** (Figure 4B), similar to apo-12′-astaxanthinal palmitate.

MS^2 fragmentation could not clarify the position of the epoxide groups, as both parent ions would result in similar fragment ions.[5,35] Therefore, further evidence for the identification of the apo-9 and apo-13 epoxide ketones was provided by the UV−vis absorption spectra. First, the epoxy-apo-13-astaxanthinone (peak 6) and its palmitate ester (peak 29) showed a blue shift of approximately 5 nm in the UV−vis absorption spectrum compared to apo-13-astaxanthinone (palmitate ester) (Figure 7A). This indicated that the conjugated system was only slightly shortened. The magnitude of the hypsochromic shift is dependent on the position of the epoxide group. Typically, a 5,6-epoxide group shortens the conjugated system with only a single double bond, whereas with a 5,8-furanoid group two double bonds are sacrificed. For intact carotenoids, epoxidation results in blue shifts of 4−13 nm for 5,6-epoxides (e.g., zeaxanthin−antheraxanthin) and blue shifts of 23−28 nm for 5,8-furanoids (e.g., zeaxanthin−mutatoxanthin).[36] For the apo-9 epoxide ketones a blue shift could not be detected due to the detection limits of the PDA detector. Although the influence of a shortened carbon skeleton of apo-astaxanthins on the magnitude of the hypsochromic shift has never been reported, the observed blue shift indicated the

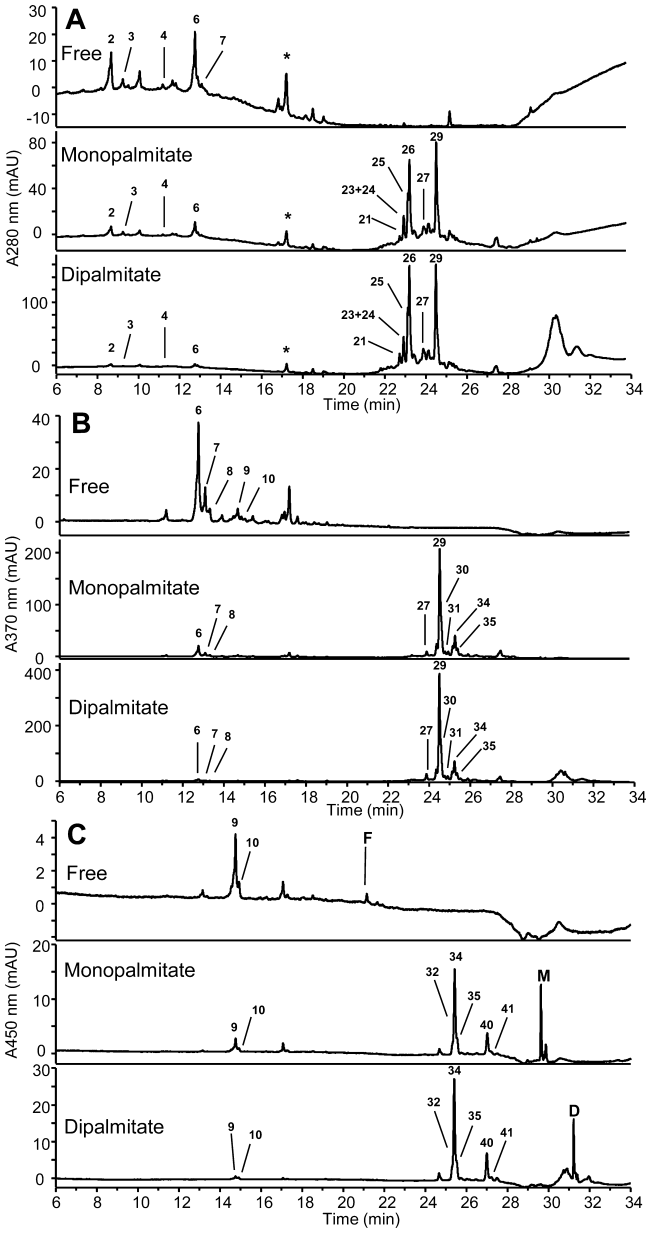

Figure 6. RP-UHPLC-UV profiles of hypochlorite-degraded free, monoester, and diester astaxanthin in methanol: (A) 280 nm; (B) 370 nm; (C) 450 nm. F, free *all-trans-* and *cis*-astaxanthin; M, *all-trans-* and *cis*-astaxanthin monoester palmitate; D, *all-trans-* and *cis*-astaxanthin diester palmitate; ∗, ghost peak.

presence of a 5,6-epoxide rather than a 5,8-furanoid group for the apo-13 epoxide (peak 29).

Acidification of the apo-astaxanthin degradation products in ethanol with 0.1 M hydrochloric acid, followed by RP-UHPLC analysis, did not lead to unambiguous annotation of the 5,6 or 5,8 configuration of the epoxide group (Figure 7B).[28] Peaks 21 and 26 (apo-9) remained intact, hinting at a 5,8-configuration. Peak 29 (apo-13) only partially disappeared, and no ketone-related new peaks appeared, hinting at either a 5,6-epoxide or a 5,8-furanoid configuration. However, for peak 29 the hypsochromic shift after acidification was only 9 nm, which might be attributed to the disappearance of apo-15-astaxanthinal palmitate (peak 30) (Figure 7B). This small hypsochromic shift would argue in favor of the 5,6-epoxide. The acidification protocol was originally designed for intact carotenoids, thus without the presence of reactive aldehyde and ketone groups as in apo-astaxanthins. All apo-astaxanthin aldehydes disappeared upon acidification, whereas the less reactive ketones partially remained. Therefore, acidification seems less suitable for distinguishing 5,6-epoxides and 5,8-furanoids in the more reactive apocarotenoids.

Epoxidation of carotenoids with HOCl might proceed as has been described for unsaturated fatty acids and cholesterol.[37] In Figure 7C this reaction is visualized as follows: the electrophilic addition of HOCl to the 5−6 CDB results in intermediate **1**. The remaining OH^- is added to either C5 or C6, resulting in chlorohydrin carotenoids (**2**). The 5,6-epoxide (**3**) or 5,8-furanoid (**4**) is subsequently formed by dehydrochlorination of **2**.[38] Additionally, the released HCl from **2** might trigger the conversion of **3** into **4**. Chlorohydrins might also be an end-point in this type of reaction,[37] but this was not the case here, as indicated by the isotope ratio of parent mass m/z 305.1 (Figure 7D). The presence of a chlorohydrin structure would have resulted in a relative intensity of 32% for the third parent mass isotope (m/z 307.1), for which only a relative intensity of 3.8% was found. This supported the formation of 5,6-epoxides or 5,8-furanoids and excluded the presence of a chlorohydrin structure.

Epoxy-apo-astaxanthinals and -astaxanthinones were also found in conjunction with reaction 1 upon light-accelerated degradation. For free astaxanthin and astaxanthin monopalmitate epoxy-apo-12′-astaxanthinal (peak 13) was annotated (Table 1). The absorbance maximum of the epoxy-apo-12′-astaxanthinal had a hypsochromic shift of approximately 20 nm compared to apo-12′-astaxanthinal. Besides apo-astaxanthins esterified with palmitate, also their epoxidized forms were found upon degradation of astaxanthin monopalmitate and dipalmitate. The palmitoyl esters of epoxy-apo-9-astaxanthinone (peak 21), epoxy-apo-15-astaxanthinal (peaks 32, 36, and 38), epoxy-apo-12′-astaxanthinal (peaks 39 and 43), and epoxy-apo-15-astaxanthinoic acid (peak 33) were all traced. The occurrence of multiple epoxides can be explained by either isomerization of the polyene backbone (*all-trans* to *cis* conversion), or the variation in 5,6-epoxide or 5,8-furanoid, or a combination thereof.

Degradation of the Fatty Acid Ester (R3). Upon examination of the diester chromatograms (Figures 3C and 6C), de-esterification was observed with especially the hypochlorite bleaching treatment, as free apo-astaxanthins (e.g., peaks 2−4 and 6−10) were formed. The de-esterification did not lead to the annotation of any new compounds and proceeded in conjunction with reaction 1 and, occasionally, reaction 2. Most probably, the de-esterification proceeded via a base-induced hydrolysis with the apo-astaxanthin as the leaving group. The reactive nucleophile in this case is likely a hypochlorite anion (OCl^-) or a hydroxide (OH^-) resulting from the HOCl. As the degradation was performed in methanol, also a methoxide anion (MeO^-) might have served as nucleophile, resulting in a fatty acid methyl ester.

For light-accelerated autoxidation, trace amounts of free astaxanthin (peak F) and astaxanthin monopalmitate (peak M) were found (Figure 3C). When the degradation was continued to 7 h, also no accumulation of free astaxanthin and astaxanthin monopalmitate was observed (data not shown). Observation of the trace amounts of de-esterification products upon light-accelerated autoxidation (e.g., a system that does not favor de-esterification) underscores the sensitivity of the analysis method employed.

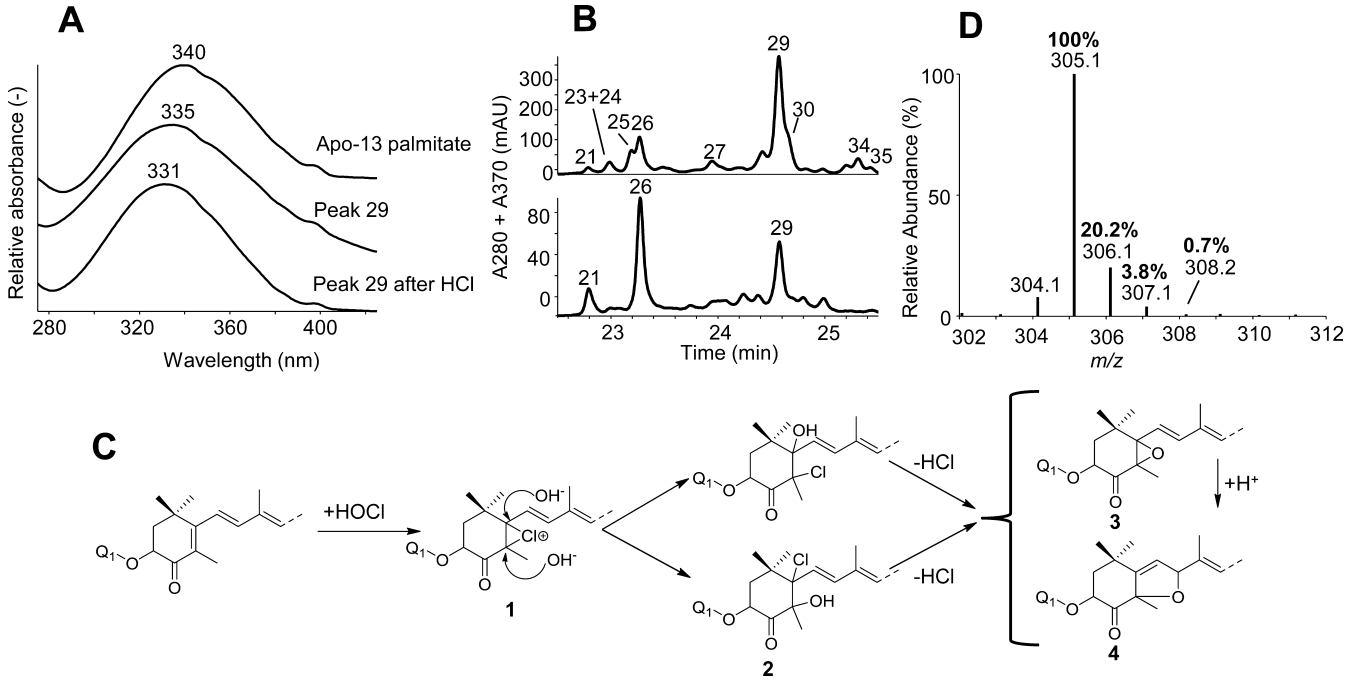

Figure 7. (A) Overlay of UV−vis absorption spectra of apo-13-astaxanthinone palmitate ester (top), epoxy-apo-13-astaxanthinone palmitate ester (middle), and epoxy-apo-13-astaxanthinone palmitate ester after acidification with HCl (bottom); (B) RP-UHPLC-UV profiles (sum of detection wavelengths 280 and 370 nm) of hypochlorite-degraded astaxanthin dipalmitate (top) and 0.1 M HCl acidified hypochlorite degraded astaxanthin dipalmitate (bottom) Numbers refer to Table 1. (C) Reaction scheme for the formation of chlorohydrins (**2**) via intermediate cloronium ion **1** and conversion to 5,6-epoxy-apo-astaxanthin (**3**) or 5,8-furanoid-apo-astaxanthin (**4**) by dehydrochlorination. Q_1 is either H or (C═O)-$C_{15}H_{31}$, (D) Full MS spectrum of epoxy-apo-13-astaxanthinone (peak 6), average of 31 spectra.

■ ASSOCIATED CONTENT

Ⓢ Supporting Information

Additional MS^2 fragmentation data of nonesterified apo-astaxanthins (Table S1) and palmitoyl apo-astaxanthins (Table S2). This material is available free of charge via the Internet at http://pubs.acs.org.

■ AUTHOR INFORMATION

Corresponding Author

*(J.-P.V.) Mail: Laboratory of Food Chemistry, Wageningen University, P.O. Box 8129, 6700 EV Wageningen, The Netherlands. Phone: +31 (0)317 482234. E-mail: jean-paul.vincken@wur.nl.

Funding

This work was supported by FeyeCon D&I and by grants from NL Agency and the Ministry of Education, Culture and Science (Project FND09014).

Notes

The authors declare no competing financial interest.

■ ABBREVIATIONS USED

HOCL, hypochlorous acid; OCl^-, hypochlorite; RP-UHPLC-PDA-ESI-MS, reversed phase ultrahigh-performance liquid chromatography with photo diode array and in-line electrospray ionization mass spectrometric detection; CDB, conjugated double bond; $[M + H]^+$, protonated parent ion; $[M + Na]^+$, sodiated parent ion

■ REFERENCES

(1) Guedes, A. C.; Amaro, H. M.; Malcata, F. X. Microalgae as sources of carotenoids. *Mar. Drugs* **2011**, *9*, 625−644.

(2) Hussein, G.; Sankawa, U.; Goto, H.; Matsumoto, K.; Watanabe, H. Astaxanthin, a carotenoid with potential in human health and nutrition. *J. Nat. Prod.* **2006**, *69*, 443−449.

(3) Miao, F.; Lu, D.; Li, Y.; Zeng, M. Characterization of astaxanthin esters in *Haematococcus pluvialis* by liquid chromatography-atmospheric pressure chemical ionization mass spectrometry. *Anal. Biochem.* **2006**, *352*, 176−81.

(4) Boon, C. S.; McClements, D. J.; Weiss, J.; Decker, E. A. Factors influencing the chemical stability of carotenoids in foods. *Crit. Rev. Food Sci. Nutr.* **2010**, *50*, 515−532.

(5) Rodriguez, E. B.; Rodriguez-Amaya, D. B. Formation of apocarotenals and epoxycarotenoids from *β*-carotene by chemical reactions and by autoxidation in model systems and processed foods. *Food Chem.* **2007**, *101*, 563−572.

(6) Stratton, S. P.; Schaefer, W. H.; Liebler, D. C. Isolation and identification of singlet oxygen oxidation products of *β*-carotene. *Chem. Res. Toxicol.* **1993**, *6*, 542−547.

(7) Marty, C.; Berset, C. Degradation products of *trans-β*-carotene produced during extrusion cooking. *J. Food Sci.* **1988**, *53*, 1880−1886.

(8) Kanasawud, P.; Crouzet, J. C. Mechanism of formation of volatile compounds by thermal degradation of carotenoids in aqueous medium. 1. *β*-Carotene degradation. *J. Agric. Food Chem.* **1990**, *38*, 237−243.

(9) Mordi, R. C.; Walton, J. C.; Burton, G. W.; Hughes, L.; Ingold, K. U.; Lindsay, D. A.; Moffatt, D. J. Oxidative degradation of *β*-carotene and *β*-apo-8′-carotenal. *Tetrahedron* **1993**, *49*, 911−928.

(10) Albrich, J. M.; McCarthy, C. A.; Hurst, J. K. Biological reactivity of hypochlorous acid: implications for microbicidal mechanisms of leukocyte myeloperoxidase. *Proc. Natl. Acad. Sci. U.S.A.* **1981**, *78*, 210−214.

(11) Hazen, S. L.; Hsu, F. F.; Gaut, J. P.; Crowley, J. R.; Heinecke, J. W. Modification of proteins and lipids by myeloperoxidase. In *Methods in Enzymology*; Lester, P., Ed.; Academic Press: New York, 1999; Vol. 300, pp 88−105.

(12) Panasenko, O. M.; Gorudko, I. V.; Sokolov, A. V. Hypochlorous acid as a precursor of free radicals in living systems. *Biochemistry (Moscow)* **2013**, *78*, 1466−1489.
(13) Norkus, E. P.; Norkus, K. L.; Dharmarajan, T. S.; Schierle, J.; Schalch, W. Serum lutein response is greater from free lutein than from esterified lutein during 4 weeks of supplementation in healthy adults. *J. Am. Coll. Nutr.* **2010**, *29*, 575−585.
(14) Granado, F.; Olmedilla, B.; Gil-Martinez, E.; Blanco, I. Lutein ester in serum after lutein supplementation in human subjects. *Br. J. Nutr.* **1998**, *80*, 445−449.
(15) Alija, A. J.; Bresgen, N.; Sommerburg, O.; Siems, W.; Eckl, P. M. Cytotoxic and genotoxic effects of β-carotene breakdown products on primary rat hepatocytes. *Carcinogenesis* **2004**, *25*, 827−831.
(16) Siems, W.; Salerno, C.; Crifo, C.; Sommerburg, O.; Wiswedel, I. β-Carotene degradation products − formation, toxicity and prevention of toxicity. In *Food Factors for Health Promotion*; Yoshikawa, T., Ed.; Karger: Basel, Switzerland, 2009; Vol. 61, pp 75−86.
(17) Handelman, G. J.; Vankuijk, F. J. G. M.; Chatterjee, A.; Krinsky, N. I. Characterization of products formed during the autoxidation of β-carotene. *Free Radical Biol. Med.* **1991**, *10*, 427−437.
(18) Sommerburg, O.; Langhans, C. D.; Arnhold, J.; Leichsenring, M.; Salerno, C.; Crifò, C.; Hoffmann, G. F.; Debatin, K. M.; Siems, W. G. β-Carotene cleavage products after oxidation mediated by hypochlorous acid − a model for neutrophil-derived degradation. *Free Radical Biol. Med.* **2003**, *35*, 1480−1490.
(19) Panasenko, O. M.; Panasenko, O. O.; Briviba, K.; Sies, H. Hypochlorite destroys carotenoids in low density lipoproteins thus decreasing their resistance to peroxidative modification. *Biochemistry (Moscow)* **1997**, *62*, 1140−1145.
(20) Lutz-Roder, A.; Jezussek, M.; Winterhalter, P. Nickel peroxide induced oxidation of canthaxanthin. *J. Agric. Food Chem.* **1999**, *47*, 1887−1891.
(21) Etoh, H.; Suhara, M.; Tokuyama, S.; Kato, H.; Nakahigashi, R.; Maejima, Y.; Ishikura, M.; Terada, Y.; Maoka, T. Auto-oxidation products of astaxanthin. *J. Oleo Sci.* **2012**, *61*, 17−21.
(22) Hayakawa, T.; Kulkarni, A.; Terada, Y.; Maoka, T.; Etoh, H. Reaction of astaxanthin with peroxynitrite. *Biosci., Biotechnol., Biochem.* **2008**, *72*, 2716−2722.
(23) Yuan, J. P.; Chen, F. Purification of *trans*-astaxanthin from a high-yielding astaxanthin ester-producing strain of the microalga *Haematococcus pluvialis*. *Food Chem.* **2000**, *68*, 443−448.
(24) Halldorsson, A.; Haraldsson, G. G. Fatty acid selectivity of microbial lipase and lipolytic enzymes from salmonid fish intestines toward astaxanthin diesters. *J. Am. Oil Chem. Soc.* **2004**, *81*, 347−353.
(25) Britton, G. Chapter 2: UV/visible spectroscopy. In *Carotenoids, Vol. 1B, Spectroscopy*; Britton, G., Liaaen-Jensen, S., Pfander, H., Eds.; Birkhäuser Verlag: Basel, Switzerland, 1995; pp 13−62.
(26) CaroteNature GmbH, Lupsingen, Switzerland, data sheet (*rac*)-12′-apo-astaxanthinal.
(27) Rivera, S. M.; Canela-Garayoa, R. Analytical tools for the analysis of carotenoids in diverse materials. *J. Chromatogr., A* **2012**, *1224*, 1−10.
(28) Eugster, C. H. Chapter 4. Chemical derivatization: microscale tests for the presence of common functional groups in carotenoids. In *Carotenoids, Vol. 1A, Isolation and Analysis*; Britton, G., Liaaen-Jensen, S., Pfander, H., Eds.; Birkhäuser Verlag: Basel, Switzerland, 1995; pp 71−80.
(29) Ghidouche, S.; Rey, B.; Michel, M.; Galaffu, N. A rapid tool for the stability assessment of natural food colours. *Food Chem.* **2013**, *139*, 978−985.
(30) Minguez-Mosquera, M. I.; Jaren-Galan, M. Kinetics of the decolouring of carotenoid-pigments. *J. Sci. Food Agric.* **1995**, *67*, 153−161.
(31) Subagio, A.; Wakaki, H.; Morita, N. Stability of lutein and its myristate esters. *Biosci., Biotechnol., Biochem.* **1999**, *63*, 1784−1786.
(32) Frassanito, R.; Cantonati, M.; Flaim, G.; Mancini, I.; Guella, G. A new method for the identification and the structural characterisation of carotenoid esters in freshwater microorganisms by liquid chromatography/electrospray ionisation tandem mass spectrometry. *Rapid Commun. Mass Spectrom.* **2008**, *22*, 3531−3539.
(33) Weesepoel, Y.; Vincken, J.-P.; Pop, R. M.; Liu, K.; Gruppen, H. Sodiation as a tool for enhancing the diagnostic value of MALDI-TOF/TOF-MS spectra of complex astaxanthin ester mixtures from *Haematococcus pluvialis*. *J. Mass Spectrom.* **2013**, *48*, 862−874.
(34) Baldas, J.; Porter, Q. N.; Leftwick, A. P.; Holzel, R.; Weedon, B. C. L.; Szabolcs, J. Mass spectrometry of carotenoid ketones. *J. Chem. Soc. D* **1969**, 415−416.
(35) Enzell, C. R.; Back, S. Chapter 7: Mass spectrometry. In *Carotenoids, Vol. 1B, Spectroscopy*; Britton, G., Liaaen-Jensen, S., Pfander, H., Eds.; Birkhäuser Verlag: Basel, Switzerland, 1995; pp 261−320.
(36) Egeland, E. S. Part VII: Data sheets aiding identification of phytoplankton carotenoids and chlorophylls. In *Phytoplankton Pigments: Characterization, Chemotaxonomy, and Applications in Oceanography*; Roy, S., Llewellyn, C. A., Egeland, E. S., Johnsen, G., Eds.; Cambridge University Press: New York, 2011; pp 665−822.
(37) Spickett, C. M.; Jerlich, A.; Panasenko, O. M.; Arnhold, J.; Pitt, A. R.; Stelmaszynska, T.; Schaur, R. J. The reactions of hypochlorous acid, the reactive oxygen species produced by myeloperoxidase, with lipids. *Acta Biochim. Polym. (Engl. Transl.)* **2000**, *47*, 889−899.
(38) Panasenko, O. M. The mechanism of the hypochlorite-induced lipid peroxidation. *BioFactors* **1997**, *6*, 181−190.